Article:
Wang, C., Murray, B.S., Bryant, M.G. et al. (2 more authors) (2025) Rheology and tribology of dextran/ polyethylene oxide-based water-in-water emulsions. International Journal of Biological Macromolecules. 148200. ISSN: 0141-8130

https://doi.org/10.1016/j.ijbiomac.2025.148200

Rheology and tribology of dextran/ polyethylene oxide-based water-in-water emulsions

Chenxi Wang[1], Brent S. Murray[1], Michael G. Bryant[2], Seunghwan Lee[3], Anwesha Sarkar[1]*

[1] Food Colloids and Bioprocessing Group, School of Food Science and Nutrition, University of Leeds, UK

[2] School of Engineering, College of Engineering and Physical Sciences, University of Birmingham, UK

[3] Institute of Functional Surfaces, School of Mechanical Engineering, University of Leeds, LS2 9JT, Leeds, UK

*E-mail: A.Sarkar@leeds.ac.uk

Highlights

- Dextran-in-polyethylene oxide (D/P) water-in-water emulsion was studied
- D/P emusions exhibit composition-dependent viscosity behaviour
- Higher P increases viscosity, more D content intensifies shear-thinning behaviour
- Emulsions exhibit speed-independent mixed lubrication (μ < 0.01) before EHL
- Droplet deformation-induced shear thinning may influence lubrication performance

Abstract

This study investigated the microstructural, rheological and tribological properties of model W/W emulsions composed of dextran (D) and poly(ethylene oxide) (P) at a fundamental level. Rheological analysis revealed that increasing the P concentration, [P], resulted in increased viscosity (η), whilst increasing the D concentration, [D], intensified shear-thinning behaviour, likely due to changes in the size of D-based droplets. Confocal laser scanning microscopy (CLSM) demonstrated a significant increase in the average droplet size with higher [D] or [P]. A striking tribological result was that the W/W emulsions demonstrated an unusual speed-independent regime, with a coefficient of friction (μ) < 0.01 over a considerable range of sliding contact speed (~10 to 100 mm s^{-1}, of physiological relevance) before the onset of the elastohydrodynamic lubrication (EHL) regime. This was not observed for solutions of the individual polymers on their own. Such composition-dependent behaviour may be due to W/W emulsion droplets entering the tribological gap, flattening and reducing the η of the entrained lubricants, thus delaying the formation of a fluid film. Overall, this detailed study shows how fabrication of W/W emulsions via phase-separating polymers can

offer unique lubrication characteristics that could provide advantageous aqueous lubricants for biomedical applications.

1.Introduction

Water-in-water (W/W) emulsions are intriguing colloidal dispersions composed of two immiscible aqueous phases, in which one phase — rich in polymer A — forms droplets that are dispersed within a continuous aqueous phase rich in polymer B [1, 2]. Unlike oil–water interfaces, the interfacial tension of water–water systems is extremely low (~0.01 mN/m) [3]. Without stabilizers, the droplet phase can persist for a considerable period (up to a few hours) due to the slow diffusion and sedimentation/creaming of the droplets — especially when the continuous phase is viscous [1, 4]. In these systems, the clean droplets with their ultralow interfacial tension and the high mobility of this interface are easily deformed and often form string-like structures under certain flow conditions [5, 6]. Additionally, these emulsions exhibit volume fraction-dependent shear-thinning behaviour even when both constituent polymers are Newtonian fluids [7]. The viscosity (η) of a lubricant is a critical parameter in tribology and most studies have focused on Newtonian fluids, which makes investigating the tribological properties of these non-Newtonian biphasic systems particularly compelling [8]. We are aware that investigations into the soft tribological properties of W/W emulsions are scarce, with only three published studies [9-11], but the mechanism of their tribological effects has not been assessed in any great detail.

Aqueous mixtures of dextran (D) and polyethylene oxide (P) is one of the most well-known polymer pairs exhibiting segregative phase separation [12, 13]. There is no issue of electrostatic interactions between D and P, and their phase behaviour has been extensively characterized in the literature, making them ideal model systems for studying W/W emulsion lubrication performance [14]. Aqueous mixtures of dextran (D) and polyethylene oxide (P) is

one of the most well-known polymer pairs exhibiting segregative phase separation [12, 13]. There is no issue of electrostatic interactions between D and P, and their phase behaviour has been extensively characterized in the literature, making them ideal model systems for studying W/W emulsion lubrication performance [14]. Furthermore, W/W emulsions composed of D and P are fully biocompatible dispersions, and their applications extend beyond theoretical studies. For example, they have been used to encapsulate adherent cells in Dulbecco's Modified Eagle Medium to generate tissue spheroids [15]. Unilamellar liposomes-stabilized D/ polyethylene glycol (PEG) emulsions have been applied as microreactors for the synthesis of $CaCO_3$ materials in biomimetic mineralization processes [16]. More recently, Wang et al. [17] reported the lubrication performance of collagen nanofibril-stabilized PEG/D emulsions, these emulsions shows promising potential as bio-lubricants for the treatment of osteoarthritis.

Particles are effective stabilizers for W/W emulsions by adsorbing to the interface [18, 19]. Although the interfacial tension in W/W systems is extremely low, the accumulation of particles at the interface can still lead to a reduction in free energy. However, it is important to note that this energy reduction is much smaller compared to O-W interfaces. To explain this phenomenon, Firoozmand et al. [20] proposed that the primary driving force for particle accumulation at the W/W interface is depletion-induced attraction, whereby particles are expelled from the polymer-rich phases and migrate toward the more solvent-rich interface. In addition to colloidal particles, triblock copolymers—comprising segments with distinct affinities for each of the two aqueous phases—can also assemble at the W/W interface to prevent droplet coalescence. Nicolai and Murray [18] suggested that such block copolymers

form polymeric micelles that adsorb at the interface and stabilize the emulsion similarly to colloidal particles. However, the presence of stabilizers of the emulsions can make the rheology and tribology much more complicated, because the deformation of droplets covered with a stabilizing layer is likely to change [21]. In this study, we use a simple system without stabilizers to isolate the intrinsic effects of droplet deformation on the overall rheological and tribological performance of the W/W emulsions.

For W/W emulsions, the viscosity ratio (λ) of the two phases, defined as the η of continuous phase divided by that of dispersed phase, is a critical parameter determining the extent of deformation of droplets [7]. It has been reported that the formation of string phases in shear flow occurs more easily when $\lambda < 1$ [7]. Therefore, we selected a formulation in which an aqueous solution of a high molecular weight P, with high η, forms the continuous phase, whilst solutions of a low molecular weight D (low η) forms the droplet phase. By limiting our scope to this single dextran-in-polyethylene oxide (D/P) emulsion system, we aim to understand if droplet deformation and string-phase formation also occurs in this system within the tribological contact zone and how this and the low viscosity droplet phase within the more viscous continuous phase influences the overall viscosity and lubrication performance.

2. Materials and methods

2.1 Materials

Dextran (D) and poly(ethylene oxide) (P) with average molecular weights of 35,000~45,000 and 200,000 Da, respectively, were purchased from Sigma-Aldrich, Dorset,

UK. Fluorescein isothiocyanate-dextran (FITC-D) with average molecular weight of 40,000 Da was also purchased from Sigma-Aldrich, Dorset, UK. MilliQ water purified by a Milli-Q apparatus (Millipore, Bedford, UK), with an electrical resistivity not less than 18.2 MΩ.cm was used as the solvent throughout the experiments. Sodium azide was used as a bactericide to prevent microbial growth.

2.2 Sample preparation

D or P were dissolved in MilliQ water and stirred overnight to obtain stock solutions. The P solution contained a small amount of insoluble particles that were removed by centrifugation at 5,000 g for 30 min. The phase diagram was determined by mixing P and D solutions at different compositions and checking for phase separation. Water-in-water (W/W) emulsion samples used for investigation were prepared by mixing required amount of the stock solutions using a vortex mixer for 1 min. **Table 1** shows the initial compositions of the pure polymer solutions and selected mixed D/P systems that phase separated into W/W emulsions as well as the volume fraction of D phase, along with the measured volume fraction of the dextran-rich phase. The phase volume fractions were determined after one week to ensure complete macroscopic phase separation. Unlike previous literature focusing purely on rheological [22] and stability assessments [12], and selecting samples along the same tie-line, W/W emulsion samples in this study were chosen within a narrow high shear viscosity window for tribological assessment.

Table 1. Nomenclature and composition of the samples.

Sample	Nomenclature	D (wt%)	P (wt%)	Volume fraction of D
Dextran (D)	4D	4	0	-
	6D	6	0	-
	10D	10	0	-
Polyethylene oxide (P)	6P	0	6	-
	8P	0	8	-
	10P	0	10	-
Water-in-water (W/W) emulsions of dextran in poly(ethylene) oxide (D/P)	1D-8P	1	8	1.8
	2D-8P	2	8	6.0
	3D-8P	3	8	12.6
	4D-4P	4	4	12.6
	4D-6P	4	6	15.2
	4D-8P	4	8	16.7
	6D-8P	6	8	23.8

2.3 Confocal laser scanning microscopy (CLSM)

A Zeiss LSM880 inverted confocal microscope (Carl Zeiss Microscopy GmbH, Germany) was used to visualize the emulsion droplets and images were analysed using ZEN Black software. A small amount (0.01 wt%) of FITC-D was added to the D stock solutions. FITC was excited at wavelength (λ) of 488 nm and the fluorescence was collected between λ ≈ 480 to 800 nm. Dark areas were therefore assumed to be unlabelled P-rich regions. The freshly prepared emulsions or pure solutions were pipetted onto a concave microscopic slide and covered with a glass coverslip before imaging. ImageJ software (version 1.54g, National Institute of Health, Bethesda, USA) was used to determine the diameter of the emulsion droplets, and the mean droplet size was calculated using at least 100 droplets in multiple images. The volume-weighted mean diameter ($D_{4,3}$) was calculated according to the

following equation:

$$D_{4,3} = \frac{\sum n_i d_i^4}{\sum n_i d_i^3}$$

where n_i represents the number of droplets with diameter d_i.

2.4 Apparent viscosity

The viscosity of samples was measured using an MCR-302 modular compact rheometer (Anton Paar, Austria). Cone and plate geometry (CP50-1) was used: cone diameter = 50 mm and cone angle = 1°. The shear rates were varied from 0.1 to 1000 s^{-1}. All experiments were carried out within 2 h of W/W emulsion formation, by which time no visible phase separation had occurred. For each measurement, 2 mL of the sample was pipetted onto the plate and a temperature-controlled cover was used to prevent evaporation and maintain the temperature at 37 ± 0.1 °C. Samples were left on the plate for 1 min to achieve thermal equilibrium before rheological measurements commenced.

2.5 Tribology

Tribological data were obtained using an MTM2 Mini Traction Machine (PCS instruments, UK) equipped with a tribo-pair consisting of smooth polydimethylsiloxane (PDMS) ball (diameter = 19 mm, Young modulus ~2.6 MPa) and disc (diameter = 46 mm). All experiments were carried out 5 minutes after W/W emulsion formation, during which time no visible phase separation occurred. A normal load (W) of 2 N, equivalent to a maximum Hertzian contact pressure of ~200 kPa [23] was used. The temperature was controlled at 37 ± 1 °C to mimic physiological conditions. The coefficient of friction (μ) was recorded for all

125 samples as a function of the entrainment speed (U) between 1 to 1000 mm s^{-1} with $U = (u_D$
126 $+ u_S)/2$, where u_D and u_S are the disc and ball speeds, respectively. The sliding rolling ratio
127 (SRR), defined as the ratio of the *absolute* value of sliding speed $| u_D - u_S |$ to U, was kept
128 constant at 0.5.

129 2.6 Statistical analysis

130 All results presented were performed in triplicate (n = 3 x 3), with samples prepared on
131 different days and mean values plotted with the standard deviation as the error bar, unless
132 otherwise stated. Statistical analyses were carried out using one-way ANOVA and multiple
133 comparison test via SPSS software and differences between samples were deemed
134 significantly different at $p < 0.05$ via Tukey's test.

135

3. Results and discussion

3.1 Phase diagrams

It is generally known that polymers P and D become incompatible at higher concentrations mainly caused by steric interactions [13, 24]. Figure 1a shows the phase diagram of the polymers used in this study, *i.e.*, D (35,000~45,000 Da) and P (200,000 Da). The curved line represents the estimated binodal curve that separates the one-phase region from the biphasic region. A homogeneous single-phase solution at the macroscopic scale is achieved when the concentrations of both components lie below this curve, as demonstrated by the CLSM images of 1D-3P and 2D-2P (Fig 1b). For compositions above this curve, the system undergoes phase separation, resulting in a polymer A-enriched phase that forms droplets dispersed in a continuous phase enriched in polymer B, as visualized in the CLSM images of P/D or D/P in Fig. 1b.

In this study, we selected phase-separated D/P with various ratios, dividing them into two groups: one group with a fixed concentration of D [D] of 4.0 wt% (4D-4P, 4D-6P, 4D-8P, as highlighted by the green line in the Fig. 1a) and the other with a fixed concentration of P [P] of 8.0 wt% (1D-8P, 2D-8P, 3D-8P, 4D-8P, 6D-8P, as highlighted by the orange line in the Fig. 1a) resulting in different overall η and volume fractions of dispersed phase, to investigate their microstructure, rheological and tribological properties.

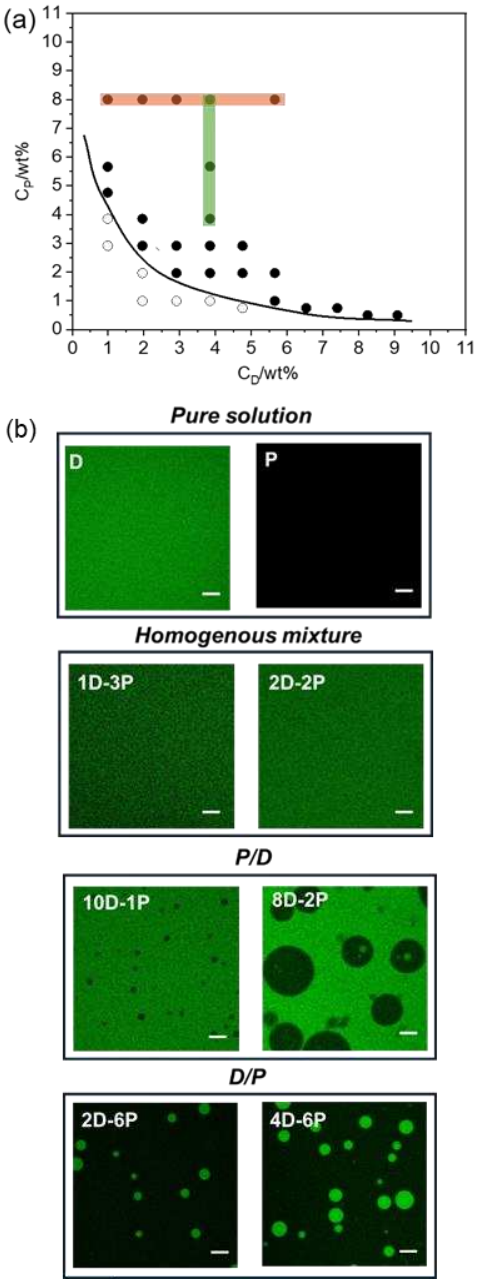

154

155 **Figure 1**. (a) Phase diagram of poly(ethylene oxide) (P) and dextran (D). Open circles
156 represent homogeneous samples, whilst closed circles indicate phase-separated samples.
157 The solid line represents the binodal curve. (b) Confocal laser scanning micrographs (CLSM)
158 of the pure D and pure P solutions, homogenous mixtures, P/D and D/P emulsions. The
159 scale bar = 20 μm.

3.2 Microstructure of W/W emulsions

The microstructure of these emulsions is in principle time dependent. All the images were captured 5 min after the preparation of the emulsions. Based on the CLSM images (Figs. 2 and 3), all the emulsions investigated are of the D/P type. Both the concentrations of D and P influence the size of droplets. One anomaly that can see is that whilst the D phase volume increases when the ratio D/P is increased (in Figure 3), as expected, in Figure 2 when more P is added keeping the D concentration constant (decreasing the D/P ratio), the volume fraction of D appears to increase. We cannot account for this other than of course sedimentation/creaming and also possibly coalescence of the droplet phase may result in different apparent volume fractions even though we tried to keep the observation times and handling of the samples the same in all instances.

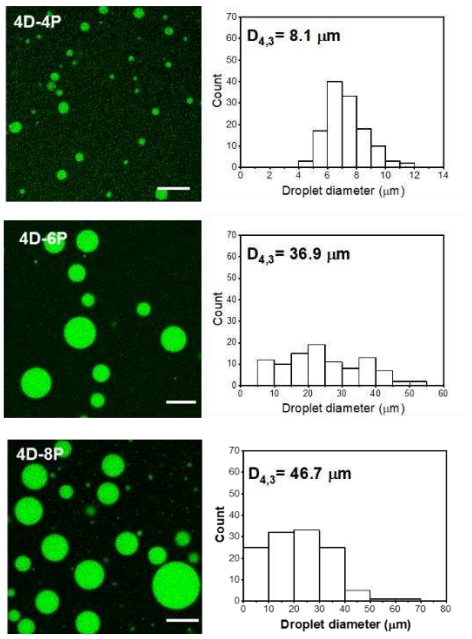

Figure 2. CLSM micrographs of W/W emulsions with a fixed concentration of D (4 wt.%) plus histograms of the droplet size distributions and corresponding D_{43} values. The scale bar = 20 μm.

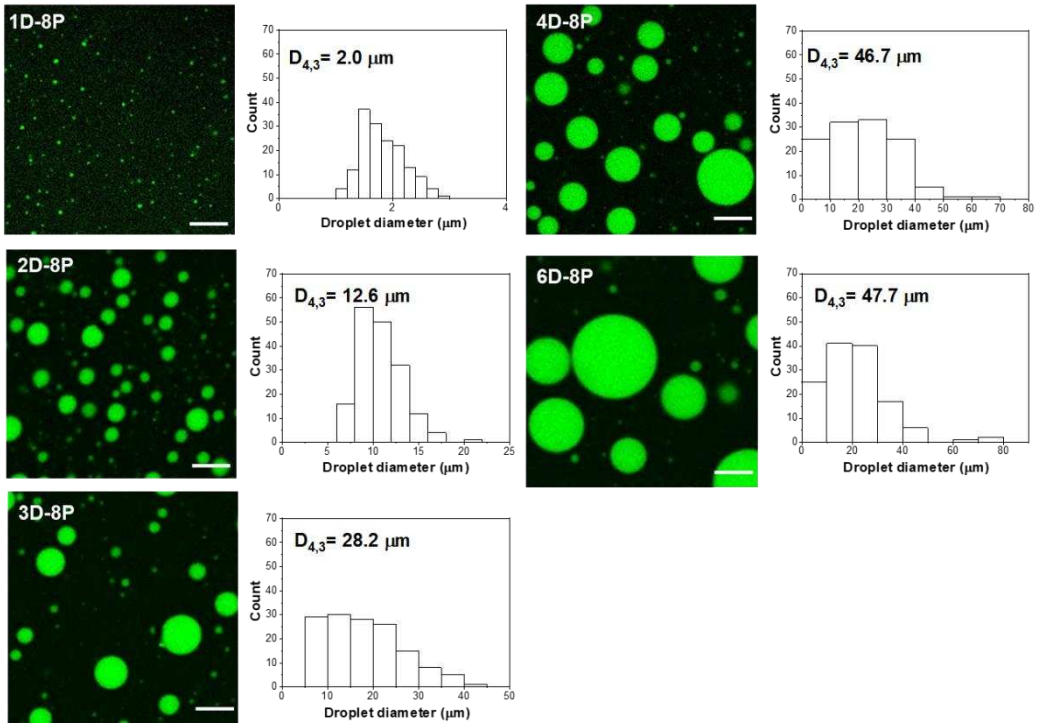

Figure 3. CLSM micrographs of W/W emulsions with fixed concentration of P (8 wt.%) plus histograms of droplet size distributions and corresponding D_{43} values. The scale bar is 20 μm.

3.3 Rheological characteristics

Figures 4a and 4b show viscosity (η) versus shear rate (γ) for pure D and P solutions at different concentrations. The pure D solutions exhibited almost Newtonian η that increased with [D], a behavior observed elsewhere [25]. The pure P solution exhibited shear-thinning behavior at high $\dot{\gamma}$ (> 100 s^{-1}), and its η was at least one order of magnitude higher than that of the D solutions of the same concentration. In Figures 5a and 5b, η versus $\dot{\gamma}$ is shown for the D/P emulsions with fixed [D] and [P], respectively. D comprises the droplet phase and P comprises the continuous phase for all these emulsions.

Of course we do not know exactly the volume factions of the dextran droplets in the P phase, nor the exact concentrations of D or P in each phase, which will vary depending on

189 the exact location of the mixed composition in the phase diagram, according to the tie-lines
190 (though it is probably safe to assume that most of the D resides in the droplet phase and
191 most of the P in the continuous phase). Accordingly, the η of the biphasic systems will
192 depend on the exact concentration of P in the continuous phase and the volume fraction of
193 droplets of D solution. If the discontinuous phase consisted of monodisperse hard spheres
194 it might be possible to predict, on theoretical grounds, the additional contribution that these
195 would make to the overall η of the continuous phase, but of course they are neither, rather
196 highly deformable fluid objects of varying sizes. At the same time, the interfacial tension will
197 also vary depending on the composition, which will determine the degree of deformation of
198 the droplets in a given shear field. (The tension will be lower the closer the composition is to
199 the binodal). However, the interfacial tension for such systems is difficult to measure and
200 indeed the exact shear rate conditions as a function of speed are also not known and our
201 objective in presenting the actual, measured η was to see how far this could account for the
202 observed tribological changes.

203 Increasing [D] and [P] increased emulsion shear-thinning behaviour, but to a varying
204 extent depending on the ratio between D and P. The shear-thinning effect is attributed to the
205 stretching out and aligning of droplets in the direction of the flow [22]. 1D-8P showed almost
206 Newtonian behaviour for $\dot{\gamma} > 60$ s^{-1}, indicating that the continuous phase dominated the
207 overall bulk η. The mean droplet radius of 1D-8P was low, with a $D_{4,3}$ of 2.05 μm, which is
208 too small to influence the structure of the emulsion under flow. Wolf and Frith (2003) reported
209 that no string phase formed in those emulsions with only 10% droplet phase volume, and
210 the flow behaviour of this polymer blend is dominated by the continuous phase [7]. In our

system, the droplet phase (D) is much less viscous than the continuous phase (P), meaning that at a fixed $\dot{\gamma}$, the high η of the continuous phase imposes substantial viscous stresses on the droplets, promoting deformation, elongation or break up. Furthermore, given the ultra-low interfacial tensions typical of W/W emulsions (~10^{-5} N/m) [26], even low $\dot{\gamma}$ generate high capillary numbers, leading to strong deformation [27].

For emulsions with constant [D] = 4 wt% and increasing [P], this resulted in intensified shear-thinning and increased η. The more pronounced shear-thinning can be attributed to the increased [P], shifting the system further from the critical point, leading to stronger phase separation and larger droplets. Larger droplets start to deform at lower $\dot{\gamma}$ keeping the interfacial tension constant. Emulsions containing a fixed [P] of 8 wt% exhibited a low shear rate plateau in their flow curves, consistent with the shear behaviour observed in the pure 8P solution (Fig. 4b), indicating that the η of the D/P emulsions was dominated by the continuous phase under at low $\dot{\gamma}$. The low shear rate plateau in η of these emulsions is higher than that of the pure 8P solution and increases significantly in emulsions with increasing [D], even though the η of pure D is very low compared to that of P. It was expected that increasing [D] results in a higher effective [P] within the continuous phase, thereby increasing the η, although the exact concentration cannot be measured in this dynamic system. Emulsions with higher [D] exhibit more pronounced shear-thinning behaviour over $\dot{\gamma}$ = 10 to 100 s^{-1} which is probably related to the droplet deformation and alignment. At high $\dot{\gamma}$ (> 100 s^{-1}), increasing [D] led to lower η, indicating that the D droplets predominantly govern the shear-thinning response at these higher $\dot{\gamma}$.

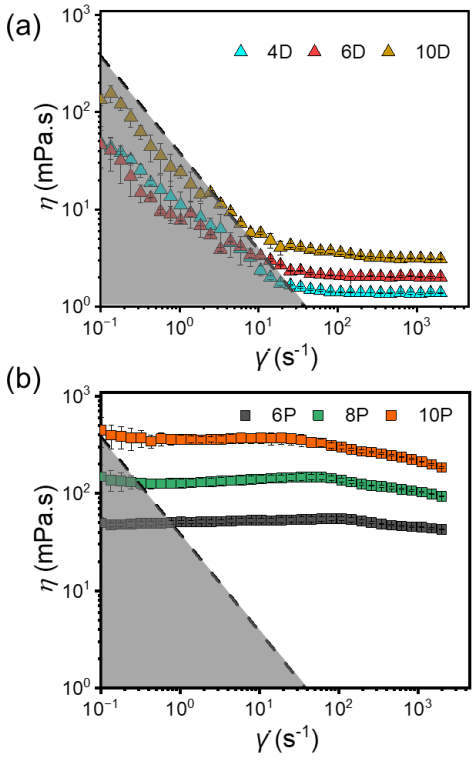

232

233 **Figure 4**. Apparent viscosity (η) versus shear rate ($\dot{\gamma}$) for (a) pure D solutions and (b) pure

234 P solutions. Data represents means and standard deviations of triplicate samples (n = 3 ×

235 3). The dashed line in (a) is the lowest measurable shear viscosity corresponding to 80×

236 the minimum measurable torque (10^{-9} N m) of our shear rheometer and the shaded region

237 denotes the invalid data range due to the geometrical limitations of the rheometer.

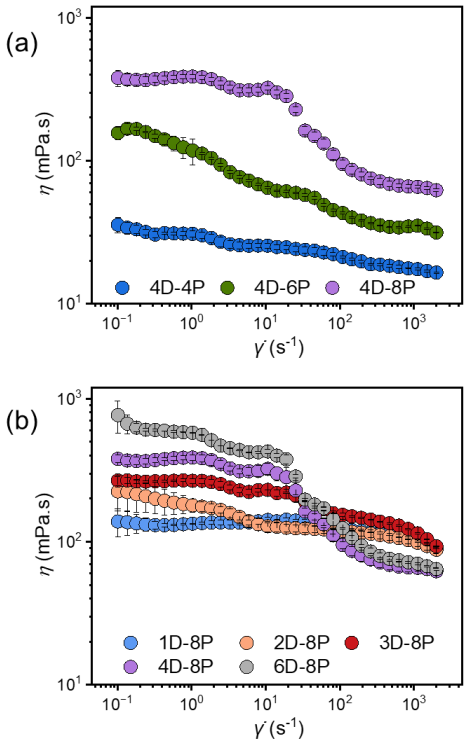

Figure 5. Apparent viscosity (η) versus shear rate ($\dot{\gamma}$) for W/W emulsions with (a) fixed concentration of D and (b) fixed concentration of P. Data represents means and standard deviations of triplicate samples (n = 3 × 3).

3.4 Tribological characteristics

3.4.1 W/W emulsions with fixed [D]

Figure 6 shows the friction results for pure D, water and D/P emulsions with fixed [D]. Fig. 6a shows that pure 4D exhibited nearly identical coefficient of friction (μ) *vs* entrainment speed (U) as water alone for the entire speed regime studied. This indicates that D molecules rarely adsorb onto PDMS surface and do not contribute to further friction lowering compared to water. Although μ decreases rapidly from approximately 30 mm/s to about 10^{-2} at 1000 mm/s, indicating a transition into a mixed lubrication regime, a further transition to an elasto-hydrodynamic lubrication (EHL) was never achieved. This behavior is attributed

to the low η of pure 4D. For 4D-4P, 4D-6P and 4D-8P emulsions, the transition to a mixed lubrication regime was observed from gradually lower speeds (within 1–10 mm s^{-1}) with increasing [P], and 4D-8P did not exhibit a distinct boundary regime. This can be attributed to the bulk viscosity; lubricants with higher η reduce friction at lower speeds because viscous fluids are more resistant to being squeezed out of the contact zone than less viscous fluids [8].

In sharp contrast, the emulsion samples displayed an unusually speed-independent mixed lubrication regime (highlighted by the green line in Fig. 6) with constant $\mu < 0.01$ over a substantial range of sliding speeds (~ 10 to 100 mm s^{-1}, which is physiologically relevant) before transitioning to the EHL regime. The entrainment rate of the lubricants depends on both U and η of fluids at the contact inlet. As U increases and the contacting gap widens due to fluid pressurization, droplets in the W/W emulsions will more easily enter the gap, where they probably flatten and reduce the effective η of the entrained lubricant, a phenomenon described as "inlet shear-thinning." [28]. To support this, the theoretical film thickness in the full-fluid film hydrodynamic regime was calculated, showing values in the range of ca. 1 to 5 μm for 4D-4P and 4D-6P, and *ca.* 3 to 10.5 μm for 4D-8P (Fig. S1). The droplet diameters observed in the emulsions (Fig. 2), ranging from 8.1 to 46.7 μm, are generally larger than the calculated lubricating film thickness. However, we propose that these droplets could still be entrained into the contact and contribute to lubrication, as they are highly deformable and can be stretched into string-like structures. This can further contribute to shear-thinning of the lubricant.

Additionally, the $\dot{\gamma}$ under the tribological contacts were estimated at different viscosities in

the calculation of the theoretical μ values. Detailed calculation procedure and results are presented in Fig. S2 and relevant discussion therein. Briefly, these calculated $\dot{\gamma}$ values (ca. 10^4 to 10^5 s^{-1}, shown in Fig. S2c and Table S1) are orders of magnitude higher than the maximum $\dot{\gamma}$ measured using the rheometer (*ca.* 10^3 s^{-1}, Fig. 5), primarily due to the much thinner film thickness under the tribological contacts compared to the 1.03 mm gap applied in rheological measurement. Thus, shear-thinning of the lubricants tends to delay the formation of a full fluid film. As [P] was increased, the speed range of this regime extended, which might be attributed to the more intense shear-thinning of the systems. This special mixed regime has been observed elsewhere for shear-thinning xanthan solutions in PDMS-PDMS ball-on-three-plates contact [29]. However, the authors focused on the EHL of the fluids and did not discuss this regime.

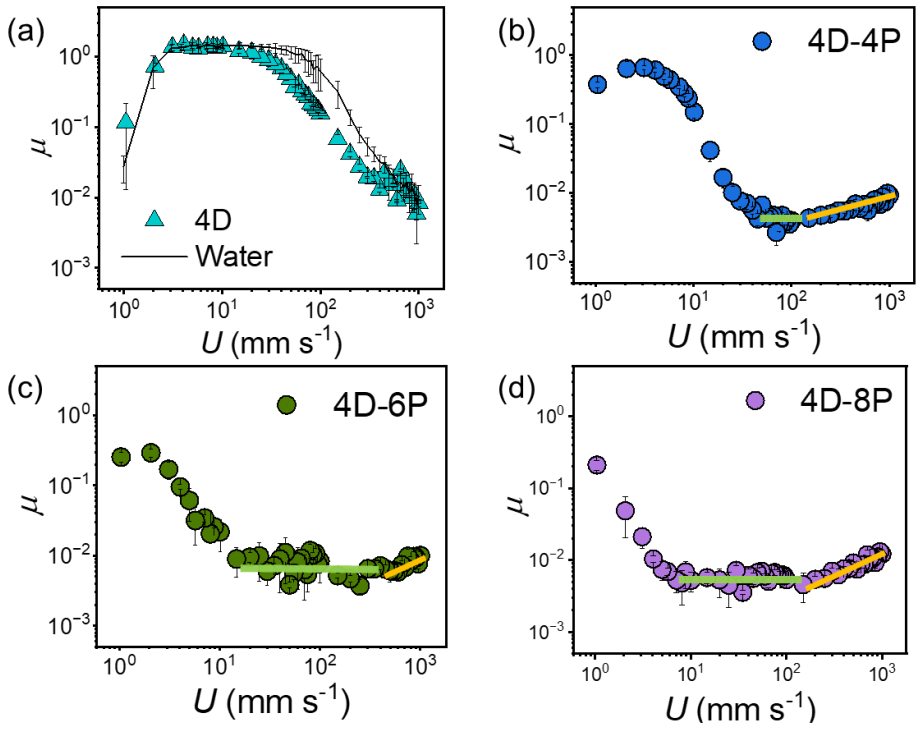

Figure 6. Coefficient of friction (μ) versus entrainment speed (U) for W/W emulsions with fixed concentration of D in PDMS-PDMS contact for 3 different mixtures: (b) 4D-4P, (c) 4D-

6P, (d) 4D-8P. The results for 4D alone and water are plotted in (a). The green line and yellow line in (b-d) show the linear fits to the mixed and hydrodynamic regimes, respectively, for the 4D-4P, 4D-6P and 4D-8P system. Data represents means and standard deviations of triplicate samples (n = 3 × 3).

3.4.2 W/W emulsions with fixed [P]

Figure 7 presents the friction data for all D/P emulsions with fixed [P], along with pure 8P and water as a control, plotted as μ versus U. Fig. 7a shows that pure 8P exhibits a classic Stribeck curve, with μ decreasing as speed increases to a minimum value, then rising again at higher speeds. The different tribological behaviour of 8P compared to 4D (Fig. 6a) is attributed to the much higher viscosity of 8P (Fig. 4). All XD-8P emulsions (X = 1, 2, 3, 4, and 6) exhibited a downward trend in μ — indicative of the mixed regime — from the lowest speeds, and no distinct boundary regime was observed. Moreover, as [D] increased, the μ values in the mixed regime gradually decreased (Fig. 8a). Stribeck curves were also constructed by multiplying the value of U by the η value in the first plateau region (specifically at $\dot{\gamma} = 3.3\ s^{-1}$) to 'eliminate' the influence of η (Fig. 8b). All samples collapsed onto a Master curve within the mixed regime, indicating that this regime is predominantly governed by the bulk phase η [30].

Similar to the 4D-XP emulsions (Fig. 5), a speed-independent mixed lubrication regime (highlighted by the green line) was also observed for XD-8P emulsions. However, with increasing [D] this special regime, characterized by invariant μ values, starts at lower U and extends over a broader range, causing the transition to the EHL regime to occur at higher

U. It has been reported that, under shear, droplets deform into string-like structures, as evidenced by images captured during shear experiments [22, 31, 32]. We propose that deformation of droplets to string phases also occurred in the D/P emulsion systems under the tribological shear. According to our film thickness calculation in Fig. S1, the calculated film thickness (*ca.* 2 to 5 μm for 6D-8P and 2~3 to 16.5 μm for the other D/P emulsions, Table S1) was 2-3 times higher than those of 4D-XP emulsions. Therefore, the likelihood of the droplets being entrained to comprise the lubricating films, although in a deformed string shape, and dominate the lubrication is even higher. Tromp and De Hoog reported that string formation in systems with higher dispersed phase volumes occurred at lower shear rates [33]. In emulsions with higher [D], the droplets are more prone to deformation and entry into the contact zone, which would cause the 'flat' mixed lubrication regime to be initiated at lower speeds and persist over a more extended range. In contrast, the 1D-8P sample displayed a μ value comparable to that of pure 8P over the entire speed range, which is consistent with the flow curve results, indicating that the small fraction of droplets had a limited effect. In the EHL regime (indicated by the orange line), the 4D-8P and 6D-8P samples exhibited significantly lower μ values than the emulsions with lower [D] *ie*.,1D-8P, 2D-8P and 3D-8P, which could be attributed to their lower η at high $\dot{\gamma}$. However, within the range of shear rates we tested (up to 2000 s^{-1}), the second plateau was not reached—the samples continued to shear thin at higher $\dot{\gamma}$ (corresponding to shear conditions in the EHL regime within the tribological contact). Therefore, scaling the Stribeck curve using the high shear η measured at 2000 s^{-1} is not appropriate. Alternatively, this phenomenon could be interpreted by the calculated μ in Fig. S2b, the η best fit the tribological data of 6D-8P and

4D-8P (10 mPa.s) are lower than those of 1D-8P, 2D-8P and 3D-8P (60 mPa.s), suggesting that droplet deformation and entrainment contribute additionally to shear thinning behaviour of the lubricants. To further clarify the tribological effect of droplets, a pure P solution (6P) with a η at high-shear rates comparable to that of 4D-8P was selected for tribological comparison (Fig. S3). 6P and 4D-8P show comparable μ values in the EHL regime due to their similar high shear rate η, whereas 4D-8P exhibits a markedly lower μ in the mixed regime. No 'flat' mixed-lubrication regime was observed for 6P. This indicates that the unique mixed-lubrication regime in D/P emulsions can be attributed to droplet deformation and entrainment within the contact.

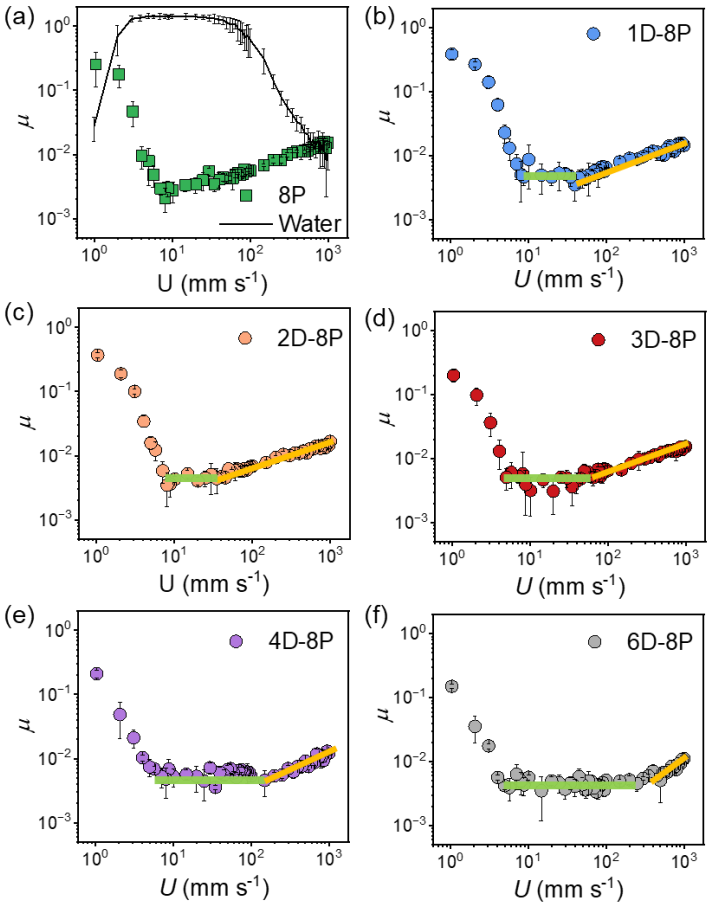

Figure 7. Coefficient of friction (μ) versus entrainment speed (U) for W/W emulsions with

fixed concentration of P (8 wt.%) in PDMS-PDMS contact: (b) 1D-8P, (c) 2D-8P, (d) 3D-8P, (e) 4D-8P, (f) 6D-8P. The results for 8P alone and water are plotted in (a) as control. The green line and yellow line in (b-f) show the linear fits to the mixed and hydrodynamic regimes for the 1D-8P, 2D-8P, 3D-8P, 4D-8P and 6D-8P system, respectively. Data represents means and standard deviations of triplicate samples (n = 3 × 3).

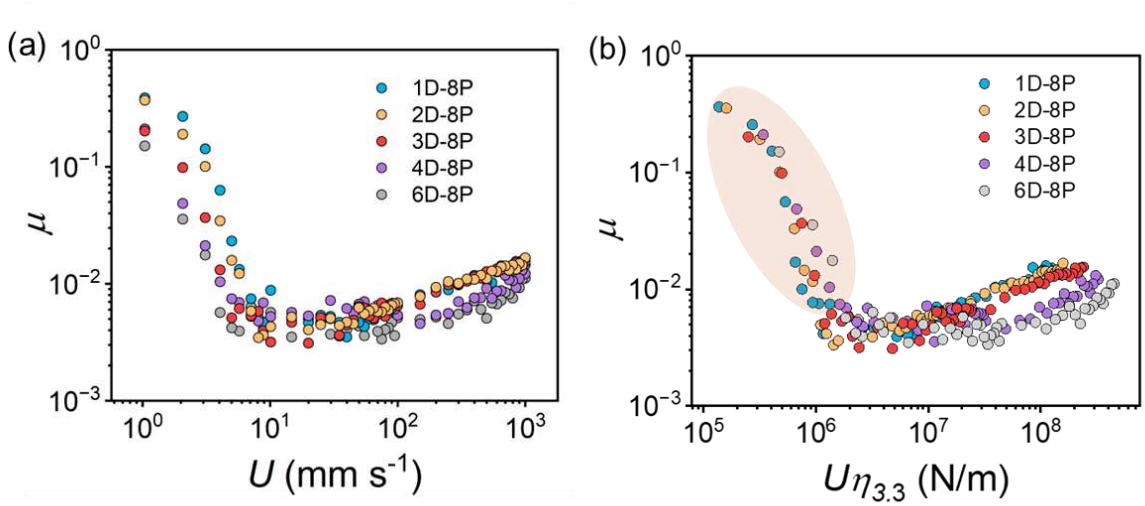

Fig. 8 Stribeck curves for D/P emulsions with [P] = 8 wt.% and variable [D] (1, 2, 3, 4 and 6 wt%) (a) as a function of entrainment speed (U) and (b) U multiplied by the viscosity measured at $\dot{\gamma} = 3.3\ s^{-1}$ ($U\eta_{3.3}$).

4. Conclusions

This study demonstrates that the microstructural, rheological, and tribological properties of W/W emulsions composed of D and P are highly sensitive to their composition. Increasing [P] primarily enhances the overall bulk viscosity, while higher [D] intensifies shear-thinning behavior by promoting larger and more deformable droplets. It is supposed that these droplets, under shear, can transform into string-like structures that enter the tribological

contact zone, thereby reducing the effective bulk viscosity and delaying the formation of a full fluid film. Most notably, the emulsions exhibited an unusually speed-independent mixed lubrication regime, with friction coefficients below 0.01 over a wide range of entrainment speed, a behavior distinctly different from that of the individual polymer solutions. The lower friction observed in emulsions with higher [D] in the EHL regime further underscores the critical role of droplet deformation in governing lubrication performance of these W/W systems. Future studies should also focus on various volume fractions of the droplets along the tie-line to see how rheology affects tribology in these biphasic systems. Overall, these findings highlight the potential of tailoring W/W emulsions via phase-separating polymers to achieve unique lubrication characteristics, offering promising avenues for the development of advanced, oil-free lubricants for biomedical applications.

Acknowledgements

The author CW acknowledges the funding from China Scholarship Council (CSC NO. 202306790025).

CRediT author statement

Chenxi Wang: Conceptualization, Project Administration, Validation, Formal analysis, Investigation, Data curation, Writing- Reviewing & Editing; Visualization; Writing- Original draft preparation, Writing- Reviewing & Editing**,** Funding acquisition**; Prof. Brent S. Murray:** Conceptualization, Methodology, Supervision, Writing- Reviewing & Editing; **Prof. Michael G. Bryant:** Supervision, Writing- Reviewing & Editing; **Dr. Seunghwan Lee:** Methodology, Supervision, Writing- Reviewing & Editing; **Prof. Anwesha Sarkar:** Conceptualization,

Methodology, Project administration; Writing- Reviewing & Editing, Supervision.

References

[1] J. Esquena, Water-in-water (W/W) emulsions, Current Opinion in Colloid & Interface Science 25 (2016) 109-119.

[2] E. Dickinson, Particle-based stabilization of water-in-water emulsions containing mixed biopolymers, Trends in Food Science & Technology 83 (2019) 31-40.

[3] D.M.A. Buzza, P.D. Fletcher, T.K. Georgiou, N. Ghasdian, Water-in-water emulsions based on incompatible polymers and stabilized by triblock copolymers–templated polymersomes, Langmuir 29(48) (2013) 14804-14814.

[4] E. Scholten, L.M.C. Sagis, E. van der Linden, Coarsening Rates of Bicontinuous Structures in Polymer Mixtures, Macromolecules 38(8) (2005) 3515-3518.

[5] J. Weiss, H. Salminen, P. Moll, C. Schmitt, Use of molecular interactions and mesoscopic scale transitions to modulate protein-polysaccharide structures, Adv Colloid Interface Sci 271 (2019) 101987.

[6] C. Wang, B.S. Murray, M. Bryant, A. Sarkar, Pickering water-in-water emulsions: A review on their rheological and tribological performance, Current Opinion in Colloid & Interface Science (2025) 101940.

[7] B. Wolf, W.J. Frith, String phase formation in biopolymer aqueous

401 solution blends, Journal of Rheology 47(5) (2003) 1151-1170.
402 [8] Y. Xu, J.R. Stokes, Soft lubrication of model shear-thinning fluids, Tribol
403 Int 152 (2020) 106541.
404 [9] Y. Wang, J. Yuan, Y. Zhao, L. Wang, L. Guo, L. Feng, J. Cui, S. Dong,
405 S. Wan, W. Liu, H. Hoffmann, K. Tieu, J. Hao, Water-in-Water Emulsions,
406 Ultralow Interfacial Tension, and Biolubrication, CCS Chemistry 4(6)
407 (2022) 2102-2114.
408 [10] K.-M. You, B.S. Murray, A. Sarkar, Tribology and rheology of water-
409 in-water emulsions stabilized by whey protein microgels, Food
410 Hydrocolloids 134 (2023) 108009.
411 [11] K.M. You, B.S. Murray, S.D. Connell, A. Sarkar, Fabrication and
412 lubrication performance of sustainable Pickering-like water-in-water
413 emulsions using plant protein microgels, Nano Select 5(4) (2024)
414 2300160.
415 [12] B.T. Nguyen, T. Nicolai, L. Benyahia, Stabilization of Water-in-Water
416 Emulsions by Addition of Protein Particles, Langmuir 29(34) (2013)
417 10658-10664.
418 [13] G. Balakrishnan, T. Nicolai, L. Benyahia, D. Durand, Particles
419 Trapped at the Droplet Interface in Water-in-Water Emulsions, Langmuir
420 28(14) (2012) 5921-5926.
421 [14] D.N.T. Nguyen, T. Nicolai, L. Benyahia, Structure and stabilization of
422 water-in-water emulsions in the presence of two types of microgels,

Journal of Colloid and Interface Science 679 (2025) 1040-1049.
[15] A.A. Das, B.W. Filby, D.A. Geddes, D. Legrande, V.N. Paunov, High throughput fabrication of cell spheroids by templating water-in-water Pickering emulsions, Materials Horizons 4(6) (2017) 1196-1200.
[16] D.N. Cacace, A.T. Rowland, J.J. Stapleton, D.C. Dewey, C.D. Keating, Aqueous emulsion droplets stabilized by lipid vesicles as microcompartments for biomimetic mineralization, Langmuir 31(41) (2015) 11329-11338.
[17] Y. Wang, J. Yuan, Y. Zhao, L. Wang, L. Guo, L. Feng, J. Cui, S. Dong, S. Wan, W. Liu, Water-in-water emulsions, ultralow interfacial tension, and biolubrication, CCS Chemistry 4(6) (2022) 2102-2114.
[18] T. Nicolai, B. Murray, Particle stabilized water in water emulsions, Food Hydrocolloids 68 (2017) 157-163.
[19] J. Esquena, Recent advances on water-in-water emulsions in segregative systems of two water-soluble polymers, Current Opinion in Food Science 51 (2023) 101010.
[20] H. Firoozmand, B.S. Murray, E. Dickinson, Interfacial structuring in a phase-separating mixed biopolymer solution containing colloidal particles, Langmuir 25(3) (2009) 1300-1305.
[21] R.B. Reboucas, N.N. Nikolova, V. Sharma, Modeling drop deformations and rheology of dilute to dense emulsions, Current Opinion in Colloid & Interface Science 77 (2025) 101904.

[22] L. Tea, T. Nicolai, L. Benyahia, F. Renou, Viscosity and Morphology of Water-in-Water Emulsions: The Effect of Different Biopolymer Stabilizers, Macromolecules 53(10) (2020) 3914-3922.

[23] A. Sarkar, E. Andablo-Reyes, M. Bryant, D. Dowson, A. Neville, Lubrication of soft oral surfaces, Current Opinion in Colloid & Interface Science 39 (2019) 61-75.

[24] M.W. Edelman, E. van der Linden, R.H. Tromp, Phase Separation of Aqueous Mixtures of Poly(ethylene oxide) and Dextran, Macromolecules 36(20) (2003) 7783-7790.

[25] V. Tirtaatmadja, D.E. Dunstan, D.V. Boger, Rheology of dextran solutions, Journal of Non-Newtonian Fluid Mechanics 97(2) (2001) 295-301.

[26] I. Norton, W. Frith, Microstructure design in mixed biopolymer composites, Food hydrocolloids 15(4-6) (2001) 543-553.

[27] A. Maestro, J.M. Gutiérrez, E. Santamaría, C. González, Rheology of water-in-water emulsions: Caseinate-pectin and caseinate-alginate systems, Carbohydrate Polymers 249 (2020) 116799.

[28] H. Spikes, Basics of EHL for practical application, Lubrication science 27(1) (2015) 45-67.

[29] K. Shahrivar, E.M. Ortigosa-Moya, R. Hidalgo-Alvarez, J. de Vicente, Isoviscous elastohydrodynamic lubrication of inelastic Non-Newtonian fluids, Tribology International 140 (2019) 105707.

[30] G.E. Yakubov, T.E. Branfield, J.H.H. Bongaerts, J.R. Stokes, Tribology of particle suspensions in rolling-sliding soft contacts, Biotribology 3 (2015) 1-10.

[31] G.B. Messaoud, E. Stefanopoulou, M. Wachendörfer, S. Aveic, H. Fischer, W. Richtering, Structuring gelatin methacryloyl-dextran hydrogels and microgels under shear, Soft Matter (2024).

[32] R. Hans Tromp, E.H.A. de Hoog, The effect of the viscosity ratio on band formation in sheared mixtures of phase-separated polymer solutions with ultralow interface tension, Molecular Physics 119(15-16) (2021) e1913253.

[33] R.H. Tromp, E.H. De Hoog, Band formation on shearing in phase-separated polymer solutions, Phys Rev E Stat Nonlin Soft Matter Phys 77(3 Pt 1) (2008) 031503.

481

Supplementary Information

Rheology and tribology of dextran/ polyethylene oxide-based water-in-water emulsions

Chenxi Wang[1], Brent S. Murray[1], Michael G. Bryant[2], Seunghwan Lee[3], Anwesha Sarkar[1]*

[1] Food Colloids and Bioprocessing Group, School of Food Science and Nutrition, University of Leeds, UK

[2] School of Engineering, College of Engineering and Physical Sciences, University of Birmingham, UK

[3] Institute of Functional Surfaces, School of Mechanical Engineering, University of Leeds, LS2 9JT, Leeds, UK

*E-mail: A.Sarkar@leeds.ac.uk

482

483

Numerical model to predict the lubricating film thickness

Based on the materials characteristics of the tribopairs and lubricants, we have firstly identified that the EHL in this study belongs to isoviscous-elastic, namely 'soft-EHL' regime [1,2]. Therefore, the lubricating film thickness could be estimated according to Equation 1. [1,2].

$$h_c = 3.28\left(U^{0.66}\eta^{0.66}E'^{-0.45}R^{0.76}W^{-0.21}\right) \quad \text{a)}$$

where η is the viscosity of the lubricant, *U* is the entrainment speed, *E'* is the reduced elastic modulus, R is the reduced radius in the entrainment direction and *W* is applied normal load. While the *E'*, *R*, and *W* are measured parameters, the viscosities, 10, 30, 60, 90 mPa.s, are estimated parameters from fitting the theoretical friction coefficient, *μ*, to the experimentally obtained *μ* vs *U* plots (Figure 6 & 7). Here, theoretical *μ* values represent the friction within the fluid in full-fluid film hydrodynamic regime (elaborated below).

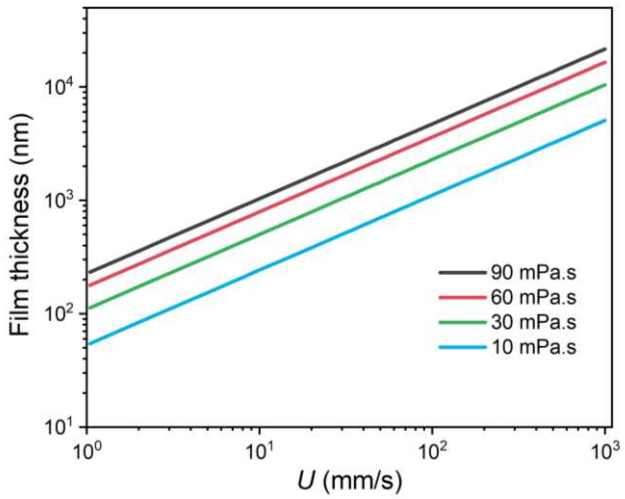

Figure S1. Calculated film thickness for PDMS-PDMS contact by applying equation 1 and effective viscosities of 10, 30, 60, 90 mPa.s.

Calculation of theoretical friction coefficient *(μ)* in full-fluid film hydrodynamic regime for PDMS- PDMS contact.

The *μ* in the hydrodynamic regime could be estimated according to the Equation 2 (where *A* is the contact area calculated with Hertzian contact equation) [2].

$$\mu = \frac{U^{0.34}\eta^{0.34}E'^{0.45}A}{3.28W^{0.79}R^{0.76}} \quad \text{b)}$$

Thus, *μ* should be linearly proportional to *U* in log-log scale. Figures S2(a) and S2(b) present

an excellent agreement between theoretical μ values and experimental values. In turn, this fitting led us to estimate effective viscosities (90, 60, 30, and 10 mPa·s) for different solution samples, including pure D, pure P solutions, and D/P emulsions with constant [D] and [P]. Lastly, based on the estimated effective viscosities, we could estimate the shear rate, $\dot{\gamma}$, in the tribological contact (Figure S2c), by applying the relation: $\dot{\gamma}$ = entrainment speed (U)/film thickness (h_c).

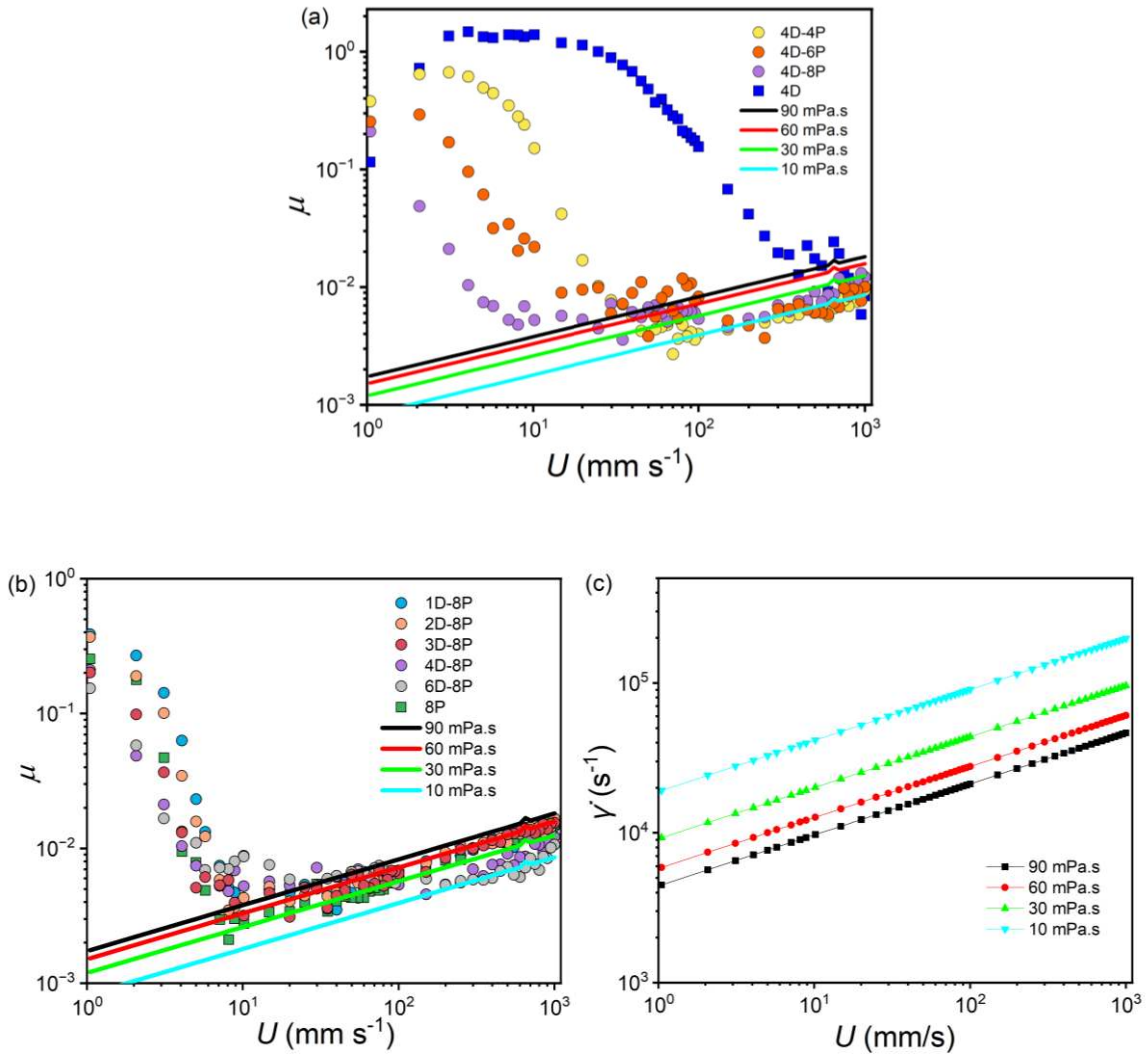

Figure S2. Stribeck curves for (a) D/P emulsions with constant [D] and pure D, and (b) D/P emulsions with constant [P] and pure P, overlaid with theoretically calculated friction coefficients (μ) based on hydrodynamic lubrication at viscosities of 10, 30, 60, and 90 mPa·s. (c) Theoretically calculated shear rates ($\dot{\gamma}$) within the PDMS–PDMS contact as a function of entrainment speed (U). The shaded region denotes the invalid data range before the full-fluid film hydrodynamic regime.

It should be noted that the film thickness calculated according to the Equation 1 is valid *in practice* only in the speed range where EHL regime is activated. This can be readily judged from the transition of μ to a linear increase in μ vs U plots in log-log scale (Figure 6, 7 or

Figure S1, S2). At lower speeds, the two surfaces are in direct contacts that the calculated film thickness is meaningless. The threshold speed that this transition occurs is different from sample to sample. Thus, the range of speed for full-fluid films for each sample and respective estimated film thickness at the lowest and highest speeds, along with the estimated viscosities, are presented in the Table S1.

Table S1. The list of fitted viscosities, $\boldsymbol{\eta}$, the minimum, $\boldsymbol{U_{mini}}$, and maximum, $\boldsymbol{U_{max}}$, speeds for the full-fluid hydrodynamic regimes, and the calculated film thickness at the respective speeds for all the emulsion samples.

Samples	Fitted η (mPa.s)	U_{mini} of full-fluid hydrodynamic regime (mm/s)	Cal. film thickness at U_{mini} (μm)	U_{max} of full-fluid hydrodynamic regime (mm/s)	Cal. film thickness at U_{max} (μm)
4D	/	/	/	/	/
4D-4P	10	100	1.11	1000	5.06
4D-6P	10	100	1.11	1000	5.06
4D-8P	30	150	2.99	1000	10.45
1D-8P	60	40	1.97	1000	16.50
2D-8P	60	45	2.14	1000	16.50
3D-8P	60	80	3.12	1000	16.50
6D-8P	10	250	2.03	1000	5.06
8P	60	8	0.69	1000	16.50

It should be also noted that the calculated film thickness could be smaller than *real* film thickness due to surface roughness of the tribopairs. However, the surface roughness (R_q) of PDMS disc is known to be less than 2 nm and that of ball is ca. 120 nm [3], whereas the film thickness is typically a few μm as shown in Table S1. Thus, the influence of surface roughness is not likely substantial.

Overall, the lubricating film thickness (Table S1) is generally smaller than the diameters of the droplets in the emulsion (8.1 to 46.7 μm, Figure 2). However, as the droplets are highly deformable, it is still possible that they are entrained into the contact zone in a deformed, string-like shape to comprise the lubricating film, especially with increasing speed.

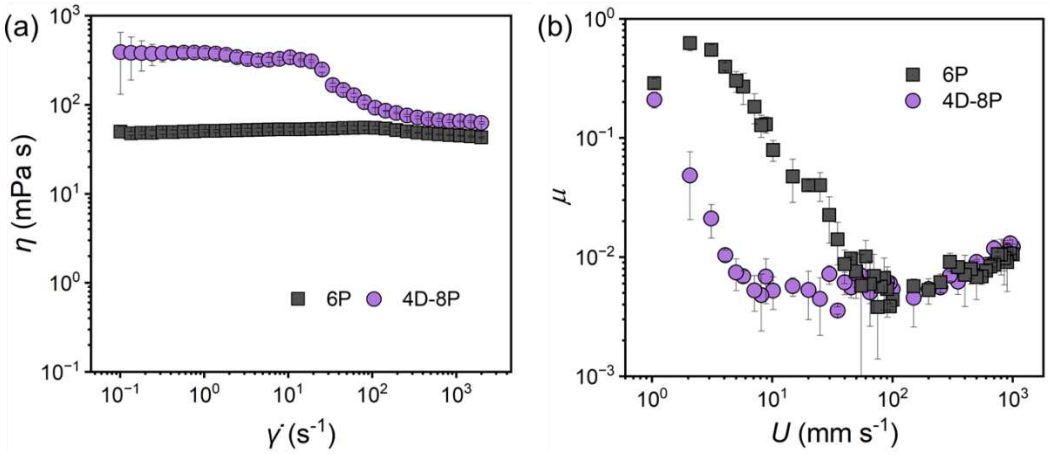

Figure S3. Apparent viscosity (η) (a) as a function of shear rate ($\dot{\gamma}$) and coefficient of friction (μ) (b) as a function of entrainment speed (U) for pure polymer (6P) and W/W emulsion (4D-8P) with comparable viscosity.

Reference:

[1] M. Esfahanian, B.J. Hamrock, Fluid-film lubrication regimes revisited. Tribol. Trans 34 (1991), 628–632.

[2] T. Røn, I.S. Chronakis, S. Lee, Lubrication of soft and hard interfaces with thermo-responsive F127 hydrogel, Polymer 55(22) (2014) 5708-5717.

[3] T. Røn, S. Lee, Influence of temperature on the frictional properties of water-lubricated surfaces, Lubricants 2(4) (2014) 177-192.